Virology 502 (2017) 73–83

Contents lists available at ScienceDirect

Virology

journal homepage: www.elsevier.com/locate/yviro

Ebola virus VP35 blocks stress granule assembly

Valerie Le Sage[a,1], Alessandro Cinti[a,b,1], Stephen McCarthy[c,d], Raquel Amorim[a,b], Shringar Rao[a,e], Gian Luca Daino[f], Enzo Tramontano[f], Donald R. Branch[c,d], Andrew J. Mouland[a,b,e,*]

[a] HIV-1 RNA Trafficking Laboratory, Lady Davis Institute at the Jewish General Hospital, Montréal, Québec, Canada H3T 1E2
[b] Department of Medicine, McGill University, Montréal, Québec, Canada H3A 0G4
[c] Centre for Innovation, Canadian Blood Services, Toronto, Ontario, Canada
[d] Department of Laboratory Medicine and Pathobiology, University of Toronto, Ontario, Toronto, Canada
[e] Department of Microbiology and Immunology, McGill University, Montréal, Québec, Canada H3A 0G4
[f] Department of Life and Environmental Sciences, University of Cagliari, Cittadella Universitaria di Monserrato, SS 554, 09042 Monserrato, Cagliari, Italy

ARTICLE INFO

Keywords:
Ebola virus
VP35
Stress granule assembly
trVLP infection
TIAR recruitment
Proximity ligation assay
In vitro GST binding assay
Poliovirus infection

ABSTRACT

Stress granules (SGs) are dynamic cytoplasmic aggregates of translationally silenced mRNAs that assemble in response to environmental stress. SGs appear to play an important role in antiviral innate immunity and many viruses have evolved to block or subvert SGs components for their own benefit. Here, we demonstrate that intracellular Ebola virus (EBOV) replication and transcription-competent virus like particles (trVLP) infection does not lead to SG assembly but leads to a blockade to Arsenite-induced SG assembly. Moreover we show that EBOV VP35 represses the assembly of canonical and non-canonical SGs induced by a variety of pharmacological stresses. This SG blockade requires, at least in part, the C-terminal domain of VP35. Furthermore, results from our co-immunoprecipitation studies indicate that VP35 interacts with multiple SG components, including G3BP1, eIF3 and eEF2 through a stress- and RNA-independent mechanism. These data suggest a novel function for EBOV VP35 in the repression of SG assembly.

1. Introduction

Ebola virus (EBOV) is a single-stranded, negative sense RNA virus of the family *Filoviridae* that produces a severe haemorrhagic fever with high mortality rates in humans and primates. The EBOV outbreak that started in 2014 was the largest registered since its discovery, with more than 28,000 cases and an estimated 50% fatality rate. In January 2016, the World Health Organization (WHO) declared the end of EBOV transmission in West Africa but noted that Guinea, Liberia and Sierra Leone remain at high risk for additional small outbreaks. EBOV can be transmitted from human to human through contact with infectious body fluids and currently there are no antiviral drugs or post-exposure prophylaxis available (Martinez et al., 2015). For these reasons, EBOV is recognized as a major threat to global health security and work is performed under biosafety level 4 containment.

An EBOV infection is characterized by an aberrant innate immune response and immunosuppression (Baize et al., 1999; Harcourt et al., 1998, 1999; Sanchez et al., 2004; Towner et al., 2004). The multi-functional protein VP35 has a critical function in innate immune evasion by preventing the phosphorylation and dimerization of interferon regulatory factor 3 (IRF-3) (Basler et al., 2003), inhibiting the induction of IFN □/□ expression (Basler et al., 2003, 2000), blocking the activation of protein kinase R (PKR) (Feng et al., 2007; Schumann et al., 2009) and suppressing RNA silencing (Fabozzi et al., 2011; Haasnoot et al., 2007). Additionally, EBOV VP35 plays crucial roles in virus replication and assembly processes (Huang et al., 2002; Johnson et al., 2006; Muhlberger et al., 1998; Noda et al., 2005). VP35 comprises an N-terminal oligomerization domain, which carries out replication/structural roles and a C-terminal interferon inhibitory domain (IID) that binds double-stranded RNA (dsRNA) and antagonizes type I IFN responses (Leung et al., 2009; Reid et al., 2005). VP35 IID acts as a binding site for NP (nucleoprotein), is able to bind the phosphate backbone of dsRNA through a central basic patch and caps the ends of dsRNA via a hydrophobic pocket. The latter two regions are distinct from each other and effectively mask the viral RNA to prevent activation of the RIG-I pathway and PKR, thus hampering induction of the host antiviral state (Kimberlin et al., 2010; Leung et al., 2009, 2010b). Moreover, VP35 can impede PKR activity and

* Corresponding author at: HIV-1 RNA Trafficking Laboratory, Lady Davis Institute at the Jewish General Hospital, Montréal, Québec, Canada H3T 1E2.
E-mail address: andrew.mouland@mcgill.ca (A.J. Mouland).
[1] V.L.S. and A.C. contributed equally to this work.

http://dx.doi.org/10.1016/j.virol.2016.12.012
Received 14 September 2016; Received in revised form 8 December 2016; Accepted 12 December 2016

consequently decrease eukaryotic initiation factor 2α (eIF2α) phosphorylation (Feng et al., 2007; Schumann et al., 2009).

To cope with stressful conditions, including heat shock, oxidative stress, nutrient deprivation or viral infection, eukaryotic cells activate cellular kinases (HRI, GCN2, PKR and PERK) to phosphorylate the initiation factor eIF2α. Phosphorylation of eIF2α impairs the formation of the eIF2-GTP-tRNA^{Met} ternary complex, which results in a rapid block to global translation. Arresting protein translation initiation causes the assembly of stress granules (SGs). SGs are dynamic accumulations of stalled translation pre-initiation complexes that are characterized by untranslated mRNAs, eukaryotic translation initiation factors (eIF4E, eIF4G, eIF4A, eIF3, eIF2), the 40S ribosomal subunit and numerous RNA-binding proteins including the poly(A) binding protein (PABP), T-cell intracellular antigen 1 (TIA-1), TIA-1-related protein (TIAR), and ras GTPase-activating protein-binding protein 1 (G3BP1) (Anderson and Kedersha, 2002; Buchan and Parker, 2009; Jain et al., 2016; Kedersha et al., 2000; Tourriere et al., 2003). SGs impart key regulatory measures on gene expression under stress conditions and consequently, viruses have evolved to co-opt components of SGs to promote their replication [reviewed in (Lloyd, 2013)]. Recently, SGs have been ascribed an important antiviral function, which requires the activity of G3BP1, in order to bridge the stress response and innate immunity (Reineke et al., 2015; Reineke and Lloyd, 2015).

As EBOV VP35 plays important roles in controlling the host innate immune response, we set out to explore whether VP35 could repress SG assembly. Indeed, we found that EBOV trVLP infection impedes SGs assembly, and that EBOV VP35 blocks the assembly of arsenite- (Ars), Pateamine A- (PatA) and selenite- (Se) induced SGs but only when the viral protein is expressed above an arbitrary concentration threshold. We demonstrate that EBOV VP35 is able to interact with several SG components, including eukaryotic elongation factor 2 (eEF2), eIF3 and G3BP1 via a stress- and RNA-independent mechanism. Furthermore, we determined that the C-terminal domain of VP35, which contains the IID and the dsRNA-binding domain, is necessary for efficient SG blockade.

2. Materials and methods

2.1. Cells, transfection and infection conditions

Green African monkey kidney (Vero) cells, human osteosarcoma-derived U2OS containing G3BP1-GFP (a kind gift from Dr. Paul Anderson, Harvard Medical School, (Ohn et al., 2008)) cells and 293 T cells (American Type Culture Collection; ATCC, Rockville, USA) were maintained in Dulbecco's modified Eagle's medium (DMEM) supplemented with 10% fetal bovine serum (FBS) (HyClone) and 1% penicillin/streptomycin (Life Technologies). Cells were transfected using JetPrime (PolyPlus transfections), according to manufacturer's instructions. Transfected cells were incubated for 24 h or otherwise indicated before being stressed, as specified below. For each experiment an average of 65% of cells were successfully transfected.

Cell-free Mahoney strain of poliovirus type 1 stocks were prepared by *de novo* infection of 293T cells followed by three freeze-thaw cycles as described in (Monette et al., 2013). Vero cells were transfected with VP35-GFP and at 24 h post-transfection, cells were washed and infected with poliovirus at an m.o.i. of 5. Titre was determined empirically to obtain 100% infection (Monette et al., 2013). At 4 h post-infection, cells were fixed and permeabilized for indirect immunofluorescence.

2.2. Plasmids

The EBOV VP35 cDNA was amplified from pCAGGS-HA-VP35(R) (Basler et al., 2003) and cloned into Myc pcDNA3.1/Zeo (MYC-VP35) and pEGFP-C1 (GFP-VP35) (generously provided by Dr. Rongtuan Lin). The VP35 truncation mutants were previously described in (Kirchdoerfer et al., 2015) (a kind gift from Dr. Erica Saphire). G3BP1-GFP was provided by Dr. Imed Gallouzi (McGill University). TIA-1-RFP was provided by Dr. Christina Vande Velde (Université de Montréal). Plasmids for the Ebola Zaire (ZEBOV) mini-genome assay (pCAGGS-NP, pCAGGS-VP35, pCAGGS-VP30, pCAGGS-L, p4cis-vRNA-RLuc, pCAGGS-T7, and pCAGGS-Tim1) were provided by Drs. Thomas Hoenen and Heinz Feldmann (NIH, NIAID, Bethesda).

2.3. Transcription- and replication-competent ZEBOV tetracistronic trVLP system

This life cycle modeling system has been previously described in (Hoenen et al., 2014; McCarthy et al., 2016). Briefly, the tetracistronic mini-genome encodes 3 of the 7 Ebola proteins (VP24, VP40 and GP1,2) and a renilla luciferase (Rluc) reporter gene. Expression plasmids for the remaining four Ebola nucleocapsid proteins (L, NP, VP30 and VP35) were also included during transfection. To produce transcription-competent virus like particles (trVLPs), 293 T cells were seeded in DMEM containing 10% FBS and transfected with the viral replication protein plasmids (L, NP, VP30, VP35), the tetracistronic Ebola mini-genome and T7 polymerase, using the CalPhos Mammalian Transfection Kit (Clontech Laboratories). After 24 h the medium was replaced with DMEM containing 5% FBS. trVLPs were harvested from the supernatant 3 days later and virus stocks were frozen at −80 °C.

For infection, Vero cells were seeded in DMEM supplemented with 10% FBS. Cells were transfected with the four viral replication protein plasmids (L, NP, VP30, VP35), as well as Tim-1, to allow efficient virus binding and entry. Eighteen hours post-transfection, media was removed and 100 μL of trVLP stock was diluted in 1.2 mL of DMEM with 5% FBS, then added to the Vero cells. At 24 and 48 h post-transfection (corresponding to 6 and 30 h after infection, respectively), cells were treated with 500 μM Ars for 1hr, then fixed and permeabilized for indirect immunofluorescence.

2.4. Stress induction

Stress was induced using 500 μM sodium Ars ($NaAsO_2$; Sigma-Aldrich) for 1 h, 300 nM PatA (a kind gift from Jerry Pelletier, McGill University) for 1 h and 1 mM sodium selenite (Na_2O_3Se; Sigma-Aldrich) for 2 h, unless otherwise stated.

2.5. Antibodies and reagents

Rabbit anti-G3BP1 (Santa Cruz Biotechnology) was used for indirect immunofluorescence microscopy at a dilution of 1:1000 and for Western blotting at a dilution of 1:10,000; mouse anti-HA (Sigma) was used for indirect immunofluorescence microscopy at a dilution of 1:1000 and for Western blotting at a dilution of 1:10,000; goat anti-eIF3 (Abcam) was used for indirect immunofluorescence microscopy at a dilution of 1:500 and for was used for Western blotting at a dilution of 1:1000; goat anti-TIAR (Santa Cruz Biotechnology) was used for indirect immunofluorescence microscopy at a dilution of 1:500; rabbit anti-Rluc (Abcam) was used for indirect immunofluorescence microscopy at a dilution of 1:500; rabbit anti-phospho-eIF2α (Ser51) (Cell Signaling Technology) was used for Western blotting at a dilution of 1:1000; mouse anti-eIF2α (Cell Signaling Technology) was used for Western blotting at a dilution of 1:1000; rabbit anti-eEF2 (Cell Signaling Technology) was used for Western blotting at a dilution of 1:1000; mouse anti-GFP (Sigma) was used for Western blotting at a dilution of 1:10,000; mouse anti-His (Santa Cruz Biotechnology) was used for Western blotting at a dilution of 1:500; mouse anti-actin (Abcam) was used for Western blotting at a dilution of 1:10,000 and mouse anti-GAPDH (Abcam) was used for Western blotting at a dilution of 1:5000. Horseradish peroxidase-conjugated secondary antibodies were from Rockland Immunochemicals and used at a

dilution of 1:5000, while AlexaFluor secondary antibodies were from Life Technologies and used at a dilution of 1:500.

2.6. Western blot analysis

Cells were lysed in NP40 lysis buffer (50 mM Tris pH 7.4, 150 mM NaCl, 0.5 mM EDTA, 0.5% NP40). Equal amounts of protein were separated by SDS-PAGE, and transferred to a nitrocellulose membrane (Bio-Rad). Membranes were probed with the indicated primary and appropriate horseradish peroxidase-conjugated secondary antibodies. Proteins were detected using Western Lightning Plus-ECL (PerkinElmer). For quantitation, the pixel intensity for each band was determined using the ImageJ program (NIH) and then normalized to the indicated control.

2.7. Indirect immunofluorescence

This method was previously described in (Vyboh et al., 2012). Briefly, cells were fixed in 4% paraformaldehyde and permeabilized with 0.2% Triton X-100. Primary antibodies were applied followed by incubation in appropriate secondary antibody. Stained cells were mounted in ProLong Gold Antifade Reagent with DAPI (Life Technologies). Laser scanning confocal microscopy was performed using a Leica DM16000B microscope equipped with a WaveFX spinning disk confocal head (Quorum Technologies) and images were acquired sequentially with a Hamamatsu ImageEM EM-charges coupled device (CCD) camera. Imaging analyses were performed by Imaris software v. 8.1.2 (Bitplane, Inc.). Confocal Z-stacks were reconstructed into 3D animations using Imaris software 3D View mode. The Surfaces function in Imaris was used to locate SGs (G3BP1 signal) and EBOV VP35 based on background subtraction and intensity thresholds. Negative isotype-matched antibody were used to control for staining specificity.

2.8. Quantification of stress granule positive cells

Twenty-four hours after transfection, cells were treated with 500 μM Ars for 1 h; 1 mM Se for 2 h or 50 nM PatA for 1 h and then processed for immunofluorescence as above. Transfected cells were identified and a SG-positive cells was defined as having at least 2 SGs as determined by colocalized G3BP1 and TIAR puncta. The observed phenotypes were representative of n =150 cells per conditions in each experiment and SGs were defined as G3BP1 foci (greater than 0.4 μm (Emara et al., 2012)). The data are presented as the percent transfected cells containing SGs.

2.9. Immunoprecipitation assay

Vero cells were transfected as described above. Briefly, after incubation without or with Ars, cells were solubilized with NP40 lysis buffer and 500 μg of protein was immunoprecipitated with anti-GFP or anti-MYC magnetic beads overnight as described by the manufacturer (MLB). To digest RNA, 10 μg/mL of RNAse A was added to the immunoprecipitation and incubated overnight at 4 °C.

2.10. In situ *protein-protein interaction assay (DuoLink®)*

G3BP1-GFP and MYC or MYC-VP35 DNA were co-transfected in Vero cells seeded on 10 mm glass coverslips in 24-well plate and were then fixed (4% PFA), permeabilized (0.05% Triton X-100 in PBS, 10 min) and incubated with antibodies. Slides were processed for *in situ* Proximity Ligation Assay (PLA) using the DUOLINK II In Situ kit (Olink), according to the manufacturer's protocol to visualize MYC-VP35/G3BP1-GFP heterodimers. Primary antibodies were mouse anti-MYC (Abcam) and rabbit anti-GFP (Clontech), which were detected using the DuoLink ® II Detection Reagent Red, Duolink® II PLA probe anti-Mouse Minus and DuoLink® II PLA probe anti-rabbit Plus. To check the specificity of the PLA signal, control experiments omitting one of the primary antibodies were performed. Imaging was performed as above. Nuclei were labeled with DAPI.

2.11. In vitro binding assay

1.5 μg of recombinant G3BP1-GST protein (Abnova) were incubated in GST SpinTrap columns (GE healthcare) for 30 min at room temperature. Columns were washed with TEN100 buffer (20 mM Tris pH 7.4, 0.1 mM EDTA and 100 mM NaCl) to remove unbound G3BP1-GST and subsequently incubated without or with 5.6 μg of recombinant His-VP35 protein (Zinzula et al., 2009) for 2 h at 4 °C. Captured complexes were washed 3 times with TEN100 buffer and elution was performed using Elution Buffer (50 mM Tris-HCl, pH8 and 10 mM glutathione). Samples were resolved by SDS-PAGE and probed using antibodies against G3BP1 and His by Western blot analysis.

3. Results

3.1. EBOV infection does not induce SG assembly

Under stressful conditions, such as viral infection, SGs play an important role in regulation of gene expression and consequently viruses have evolved to co-opt SGs components to promote their own replication and eliminate antiviral responses (Poblete-Duran et al., 2016). We set out to determine whether or not EBOV infection trigger the assembly of SGs, however, work with EBOV is restricted to BSL4 containment. A recently developed transcription- and replication-competent virus-like particle (trVLP) system has made it possible to study the EBOV life cycle under BSL2 conditions (Hoenen et al., 2014; Watt et al., 2014). Vero cells were infected, as described in material and methods, and SG assembly was evaluated by immunofluorescence. In trVLP-infected cells, 8% of cells displayed SG assembly, which was comparable to the 10% of uninfected cells with SGs (Fig. 1A and B). Interestingly the SG marker TIAR-1 was found to colocalize with VP35 in the viral inclusions. Oxidative stress inducing agents such as Ars induce rapid SG assembly through the phosphorylation of eIF2α (Kedersha et al., 1999; Ohn et al., 2008). As expected, the addition of sodium arsenite (Ars) increased to 80% the amount of uninfected cells having SGs, whereas only 37% of trVLP-infected cells demonstrated SG assembly (Fig. 1A and B). These results indicate that EBOV-trVLP infection does not induce SG assembly and suggest that EBOV has evolved a mechanism by which to block the assembly of SGs.

3.2. EBOV VP35 blocks SG assembly

SGs are associated with silenced transcripts and many viruses are known to subvert the function of these RNA granules for their replicative advantage. As EBOV VP35 counteracts many cellular antiviral activities, we investigated whether EBOV VP35 would interfere with cellular SG assembly. We transfected African green monkey kidney Vero cells with GFP or GFP-VP35-expressing plasmids and did not treat or exposed to stress with sodium arsenite (Ars) and SG assembly was monitored by indirect immunofluorescence of G3BP1 and TIAR. In the absence of stress, 11.8% and 1.5% of GFP- and GFP-VP35-transfected cells showed SG assembly, respectively (Fig. 1C and D). In GFP-transfected Vero cells, Ars treatment induced abundant SG assembly in 73.6% of cells, as demonstrated by colocalization of G3BP1 and TIAR in cytoplasmic foci of greater than 0.4 μm (Fig. 1C and D). In VP35-expressing cells treated with Ars, TIAR was observed to have shuttled from the nucleus to the cytoplasm but only accumulated in SG foci that colocalized with G3BP1 in 23% of cells (Fig. 1C and D).

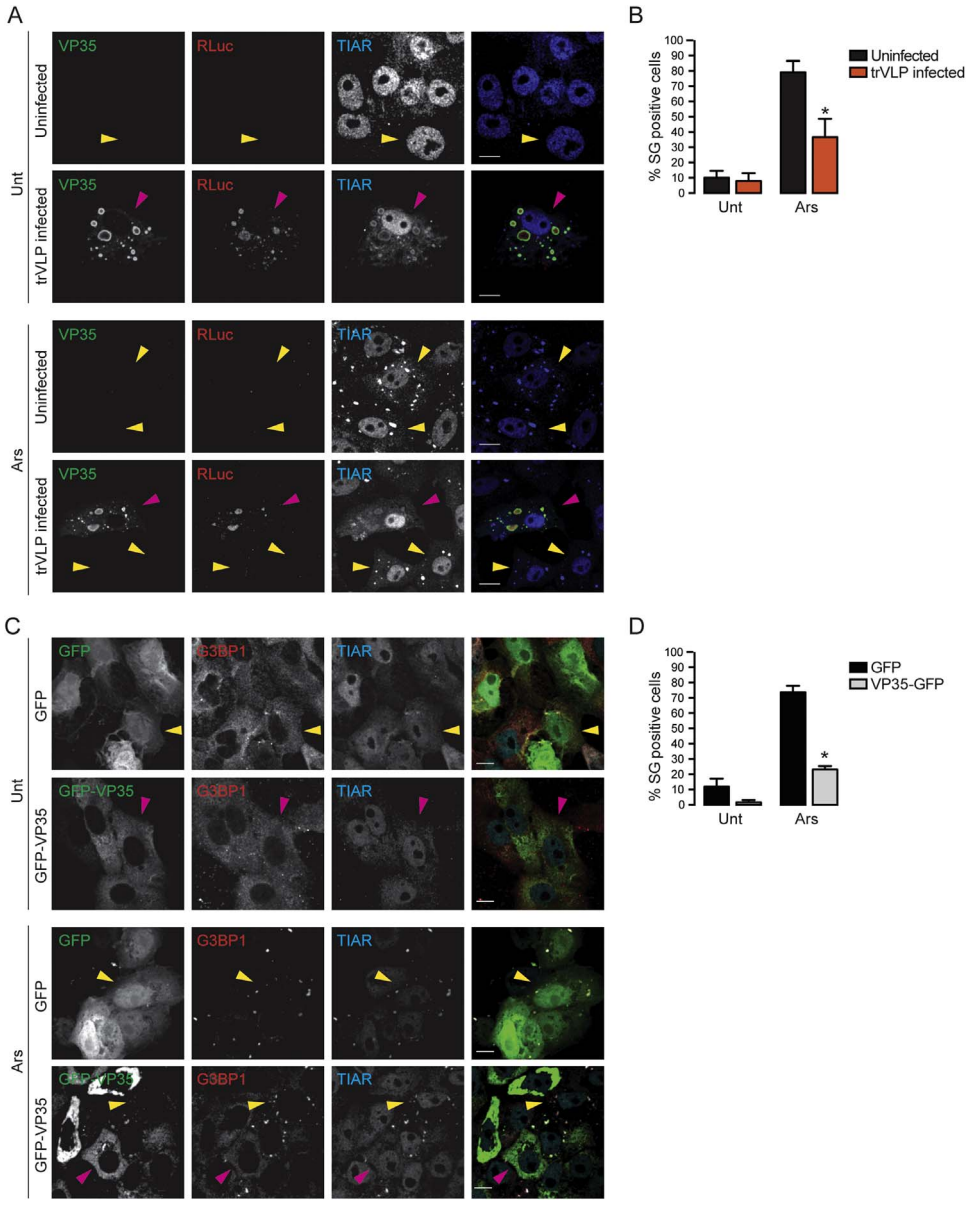

Fig. 1. EBOV blocks SG assembly. (A) Vero cells were infected, as described in material and methods, and 30 h after were left untreated or treated with 500 μM Ars for 45 min. Yellow arrowheads indicate ZEBOV-negative cells, while pink arrowheads show ZEBOV-expressing cells. Scale bars are 10 μm. (B) Quantification of uninfected or trVLP-infected Vero cells containing SGs from Panel 1 A. Error bars represent the standard deviation from three independent experiments with at least 50 cells counted per treatment. Asterisks represent statistically significant difference between uninfected and trVLP-infected cells (Two-way ANOVA; $p < 0.001$). (C) Vero cells transfected with GFP or GFP-VP35 were untreated or incubated with 500 μM Ars for 45 min. Cells were stained for G3BP1 (red) and TIAR (cyan). Yellow arrowheads indicate VP35-negative cells, while pink arrowheads show VP35-expressing cells. Scale bars are 10 μm. (D) Quantification of GFP- or GFP-VP35-transfected Vero cells containing SGs from Panel 1 C. Error bars represent the standard deviation from three independent experiments with at least 150 cells counted per treatment. Asterisks represent statistically significant difference between GFP and GFP-VP35-expressing cells (Two-way ANOVA; $p < 0.001$).

3.3. EBOV VP35 blocks SG assembly independent of eIF2α phosphorylation

PKR and other kinases phosphorylate eIF2α to block translation initiation and regulate SG assembly (Kedersha et al., 1999; Ohn et al., 2008). Because EBOV VP35 inhibits activation of PKR (Feng et al., 2007; Schumann et al., 2009), we examined the phosphorylation status of eIF2α in untreated and Ars treated cells expressing GFP-VP35. Protein lysates were analyzed by Western blot using an antibody specific for eIF2α phosphorylation at S51. As shown in Fig. 2A, very little phosphorylation of eIF2α was detected in untreated cells expressing GFP with a slight decrease in phospho-eIF2α being consistently observed in GFP-VP35-transfected cells (Fig. 2A, lanes 1 and 2, and B). As expected, high levels of eIF2α phosphorylation (2.7-fold increase) were observed in extracts of GFP-expressing cells treated with Ars (Fig. 2A, lane 3). A similar 3.1-fold increase in the levels of phospho-eIF2α was detected in Ars stressed cells transfected with GFP-VP35 (Fig. 2A, lane 4, and B) as compared to untreated (Fig. 2A, lane 2, and B). The amount of total eIF2α remained constant under all conditions tested (Fig. 2A).

To confirm the ability of EBOV VP35 to block SG assembly independently of eIF2α phosphorylation, we treated the cells with Pateamine A (PatA). PatA treatment induces SG assembly via an eIF2α-independent mechanism by blocking translation initiation through the hyperactivation of the eIF4A helicase, which disrupts the eEF4F complex (Dang et al., 2006). GFP- or GFP-VP35-transfected Vero cells were untreated or exposed to PatA and SG assembly was monitored by indirect immunofluorescence of G3BP1 and TIAR.

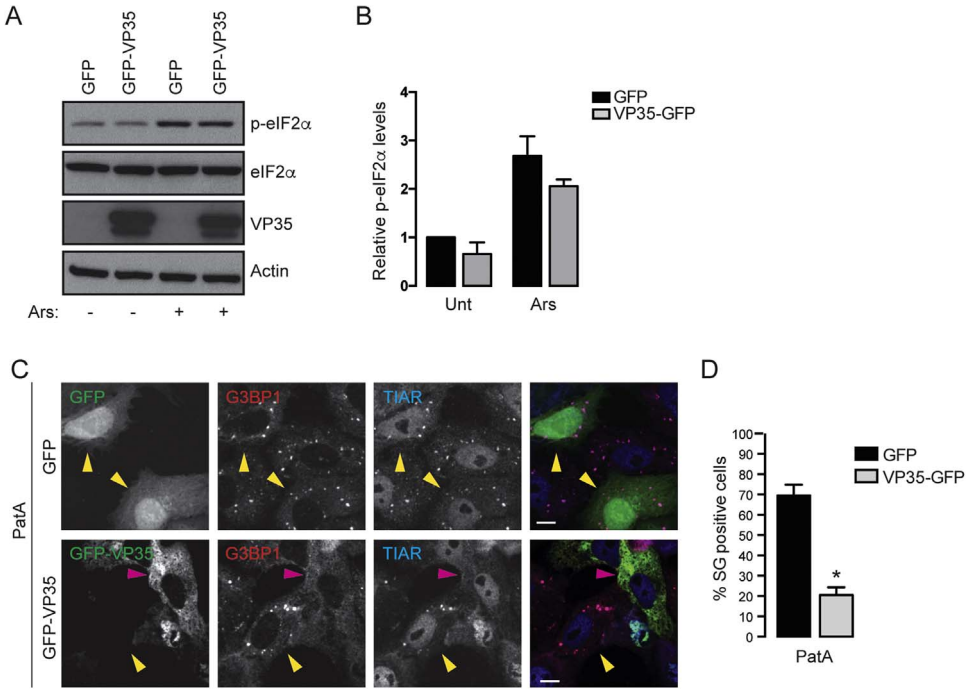

Fig. 2. EBOV VP35 blocks SG assembly independent of eIF2α phosphorylation. (A) Vero cells were transfected with GFP or GFP-VP35 and stressed without or with 500 μM Ars for 1 h. Cell lysates were subjected to SDS-PAGE, immunoblotted and probed with the indicated antibodies. (B) Densitometry quantification of phospho-eIF2α was determined by ImageJ analysis. Values presented in the graph are normalized against the total amount of eIF2α in the cell lysate and represent fold change with the untreated GFP-transfected cells being arbitrarily set to 1. (C) Vero cells transfected with GFP or GFP-VP35 were untreated or incubated with 50 nM PatA for 1 h. Cells were stained for G3BP1 (red) and eIF3 (cyan). Yellow arrowheads indicate VP35-negative cells, while pink arrowheads show GFP-expressing cells. Scale bars are 10 μm. (D) Quantification of cells exhibiting SGs derived from results shown in Panel 2 C. Error bars represent the standard deviation from three independent experiments with at least 150 cells counted per treatment. Asterisks represent statistically significant difference between GFP and GFP-VP35-expressing cells (Two-way ANOVA; $p < 0.001$).

Similarly to Ars-treated cells (Fig. 1C and D), in PatA-treated cells expressing GFP-VP35, SGs were observed in 21.5% of cells, as compared to 69% of GFP-expressing cells having SGs (Fig. 2B and C). Taken together, these results indicate that the VP35-mediated SG blockade occurs via an eIF2α-independent mechanism.

3.4. EBOV VP35 blocks non-canonical SG assembly

Sodium selenite (Se), the commercially available version of selenium, causes mRNA translational repression followed by the assembly of non-canonical type II SGs, which differ in size, localization, composition (lack of eIF3) and mechanism of assembly from those induced by Ars (Fujimura et al., 2012). We examined the ability of VP35 to block the accumulation of non-canonical Se-induced SGs. Osteosarcoma U2OS cells stably expressing GFP-G3BP1 (Ohn et al., 2008) were mock- (pcDNA3.1) or MYC-VP35-transfected and subsequently stressed without or with Se. In untreated cells, 6% and 4.3% of mock and MYC-VP35 transfected cells displayed SG, respectively (Fig. 3A and B). As expected, Se treatment resulted in 73.4% of mock-transfected cells being positive for SG assembly, whereas only 8.5% of MYC-VP35-expressing cells had SGs (Fig. 3A and B). To further investigate the ability of VP35 to block the assembly of SGs induced by other viral infection, we monitored the SGs formation induced by Poliovirus (PV). In fact, it has been proposed that the cleavage of eIF4G by the viral protease 2A is the main mechanism by which PV induces SG assembly at early times during infection (Dougherty et al., 2015). Vero cells were transfected with VP35-GFP and 24 h later infected with the Mahoney strain of poliovirus type 1. 4 h post-infection the assembly of SGs was monitored by indirect immunofluorescence of TIAR. As shown in Supp. Fig. 1, TIAR aggregates into cytoplasmic puncta in both VP35-GFP positive and negative cells, indicating that VP35 is not able to counteract poliovirus-triggered SG assembly. Taken together these results indicate that EBOV VP35 blocks non-canonical SG assembly but not those induced by PV infection.

3.5. A threshold level of EBOV VP35 is required to block SG assembly

To better understand the kinetics of the VP35-induced SG blockade, we examined the assembly of SGs overtime. In untreated cells, as expected, no SGs were visible and TIAR was predominantly localized to the nucleus (Taupin et al., 1995), while GFP-VP35 was diffusely distributed within the cytoplasm throughout the duration of the time course (Supp. Fig. 2). Western blot analysis using an antibody against GFP confirmed that expression of GFP and GFP-VP35 increased over time (Fig. 4B). At 3 h post-transfection the distribution of VP35, expressed at detectable levels only in few cells, appeared punctate and colocalized with SGs in the presence of Ars with 85.5% of GFP-VP35 positive cells harbouring SGs (Fig. 4A and C). 79.5% of GFP-VP35 expressing cells were positive for SGs after 6 h (Fig. 4A and C). At 12 h post-transfection, the number of cells containing SGs further decreased to 37.2% as the concentration of GFP-VP35 continued to increase (Fig. 4A and C). After reaching a threshold of VP35 expression, the percentage of cells containing SGs significantly dropped to 17.2% at 24 h and GFP-VP35 appeared diffusely cytoplasmic (Fig. 4A and C). These data indicate that EBOV VP35 requires a threshold of viral protein expression to block SGs assembly.

3.6. EBOV VP35 interacts with SG components

Many viruses have evolved to disrupt RNA granules through the cleavage of key host factor, the manipulation of PKR activation or redirecting SG components (Tsai and Lloyd, 2014). To begin the characterization of a possible mechanism behind EBOV-mediated SG blockade, we co-transfected Vero cells with G3BP1-GFP or TIA-1-HA and MYC or MYC-VP35 and cell lysates were immunoprecipitated

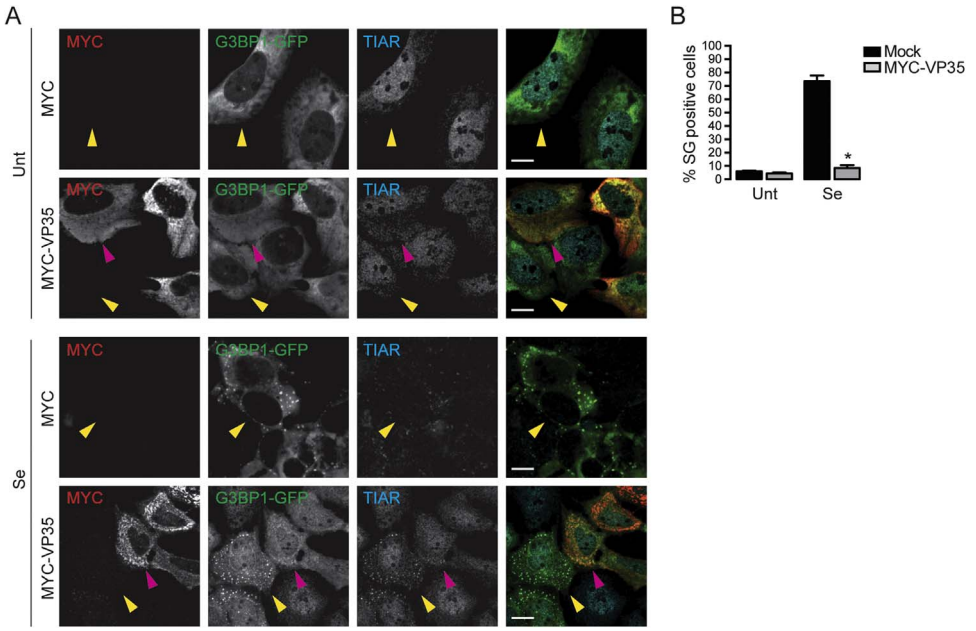

Fig. 3. EBOV VP35 blocks Se-induced SGs. (A) U2OS GFP-G3BP1-expressing cells transfected with pcDNA3.1 or MYC-VP35 were untreated or incubated with 1 mM Se for 2 h. Cells were stained for TIAR (blue) and VP35 (red). Yellow arrowheads indicate VP35-negative cells, while pink arrowheads show VP35-expressing cells. Scale bars are 10 μm. (B) Quantification of cells exhibiting SGs derived from results shown in Panel 3 A. Error bars represent the standard deviation from three independent experiments with at least 150 cells counted per treatment. Asterisks represent statistically significant difference between mock or MYC-VP35-expressing cells in the presence of Se (Two-way ANOVA; $p < 0.001$).

using anti-MYC antibodies. G3BP1-GFP, but not TIA-1-HA, was pulled down with VP35 (Fig. 5A). Additionally, eEF2 and eIF3 were found to exclusively associate with MYC-VP35 and not the tag alone (Fig. 5A). Overexpression of many SG-associated proteins, including TIA-1/TIAR and G3BP1 induce the spontaneous SG assembly in the absence of additional stress (Gilks et al., 2004; Tourriere et al., 2003). We determined that VP35 was able to block the assembly of TIA-1-RFP or G3BP1-GFP induced SGs (Fig. 5B and C).

To evaluate whether VP35 is capable to associate with SG components in the absence of stress signals, co-immunoprecipitation experiments were performed with lysates prepared from GFP- or GFP-VP35-transfected Vero cells in the presence and absence of Ars stress using anti-GFP beads. As shown in Fig. 5D, we demonstrated that the SG components, eEF2, eIF3 (Jain et al., 2016) as well as G3BP1, interacted with GFP-VP35 but not GFP alone, regardless of the absence or presence of Ars stress. Additionally, the interactions were not dependent upon RNA, as eEF2, eIF3 and G3BP1 still co-immunoprecipitated in the presence of RNAse (Fig. 5D).

All together these results indicate that EBOV VP35 is capable of associating with a number of SG components regardless of an external stress or RNA, and supports the hypothesis that VP35 blocks SG formation by recruiting fundamental SG components.

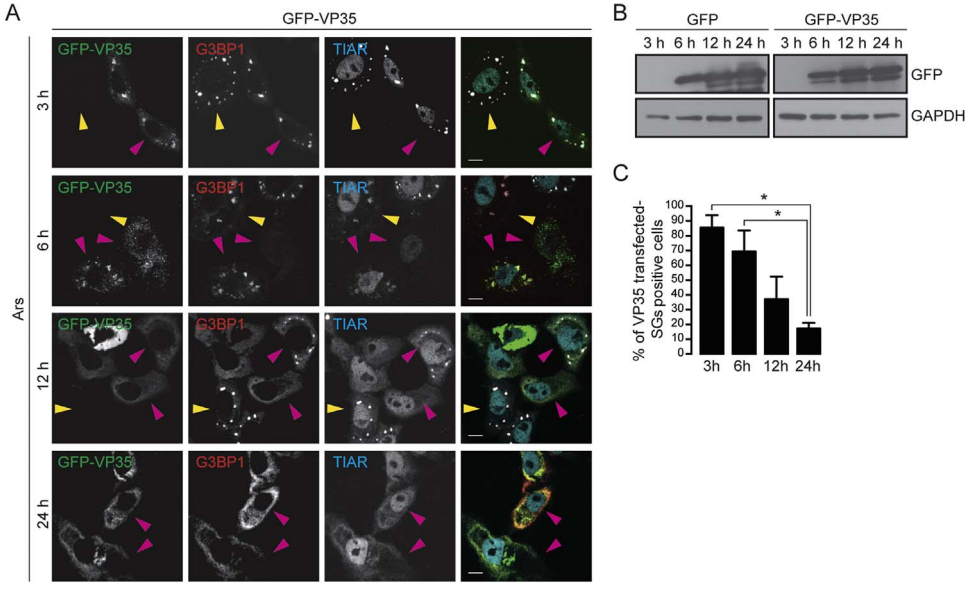

Fig. 4. Blockade of Ars-induced SGs requires a threshold concentration of GFP-VP35. (A) Vero cells were transfected with GFP or GFP-VP35 for the indicated times and treated with 500 μM Ars for 1 h before fixation. Cells were stained for SGs using antibodies against G3BP (red) and TIAR (cyan). Yellow arrowheads indicate VP35-negative cells, while pink arrowheads show VP35-expressing cells. Bar, 10 μm. (B) Cell lysates from Vero cells transfected with GFP or GFP-VP35 were collected at the indicated times. Western blot analysis was preformed with antibodies against GFP and GAPDH. (C) Quantification of cells exhibiting SGs derived from results shown in Panel 4 A. Error bars represent the standard deviation from three independent experiments with at least 150 cells counted per treatment. Asterisks represent statistically significant difference between early times (3 and 6 h) post-transfection and 24 h post-transfection (Two-way ANOVA; $p < 0.001$).

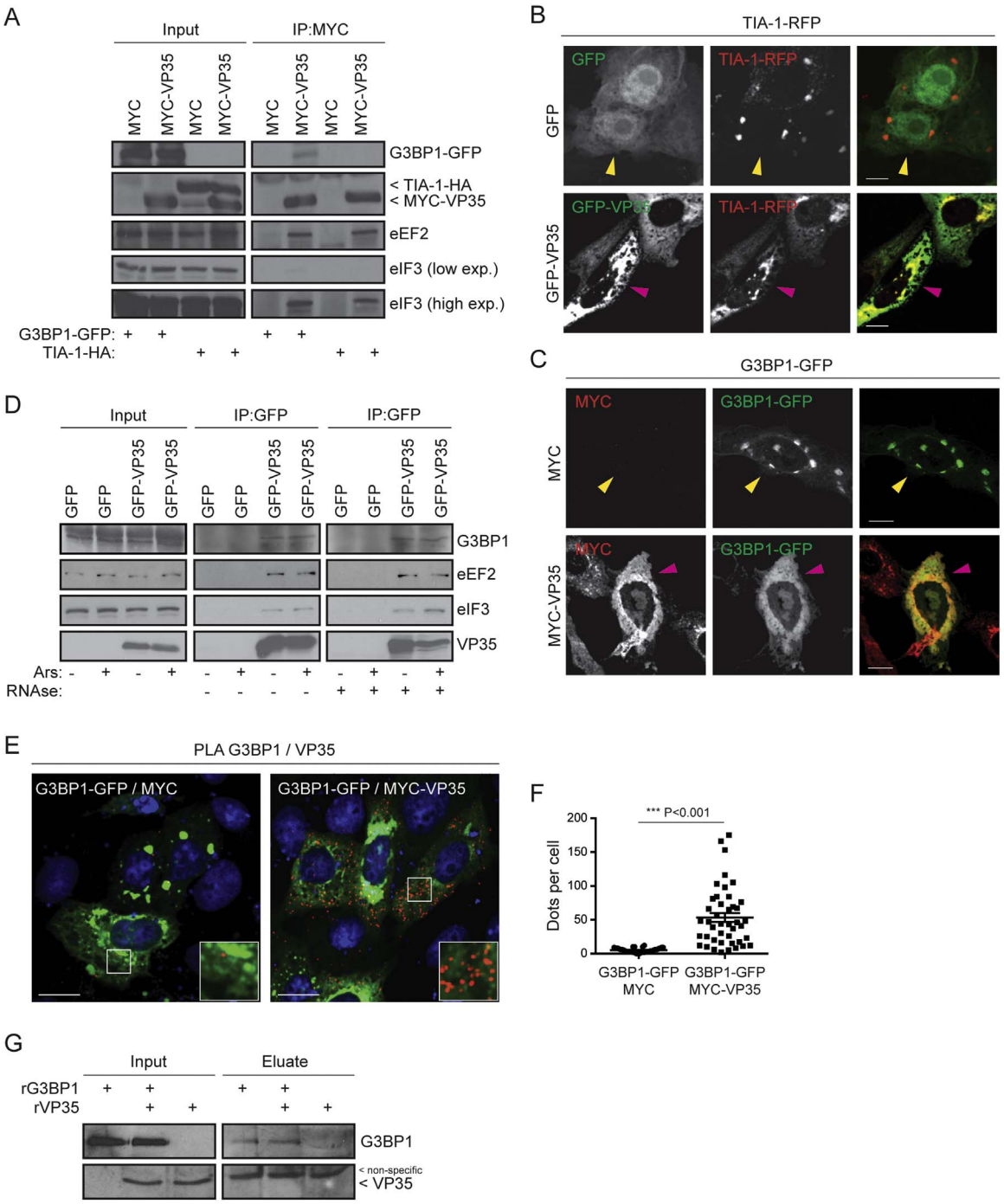

Fig. 5. EBOV VP35 interacts with multiple SG components. (A) Vero cells were transfected with G3BP1-GFP or TIA-1-HA and MYC or MYC-VP35 for 24 h. Cell lysates were collected and subjected to anti-MYC immunoprecipitation. VP35-associated proteins were processed for Western blotting and probed for GFP, HA, MYC, eEF2 and eIF3. Data shown is representative of three independent experiments. (B) Vero cells were transfected with TIA-1-RFP and GFP or GFP-VP35 for 24 h. Yellow arrowheads indicate VP35-negative cells, while pink arrowheads show GFP-expressing cells. Scale bars are 10 μm. (C) Vero cells were transfected with G3BP1-GFP and MYC or MYC-VP35 for 24 h. Yellow arrowheads indicate VP35-negative cells, while pink arrowheads show MYC-expressing cells. Scale bars are 10 μm. (D) Vero cells were transfected with GFP or GFP-VP35 and left untreated or treated with 500 μM Ars for 1 h. Cell lysates were collected and subjected to anti-GFP immunoprecipitation in the absence of presence of RNAse A. VP35-associated proteins were processed for Western blotting and probed for GFP, eEF2, eIF3 and G3BP1. Data shown is representative of three independent experiments. (E) G3BP1-GFP and MYC or MYC-VP35 co-transfected Vero cells were fixed, permeabilized, and incubated with anti-mouse MYC and anti-rabbit GFP. MYC-VP35/G3BP1-GFP heterodimers were visualized through incubation with PLA probes. Each red dot corresponds to a single interaction event between VP35 and G3BP1. Nuclei were stained with DAPI (blue). Images shown are representative of at least 60 cells. (F) The graph indicates the number of spots per cell ± SEM from E. Asterisks represent statistically significant difference (unpaired *t*-test; $p < 0.001$). (G) GST-G3BP1 was incubated with GST SpinTrap columns in the presence of absence of VP35-HIS. After washing extensively, the proteins bound to the beads were detected by Western blotting analysis using anti-G3BP1 and anti-HIS antibodies.

Considering that different viruses interact with G3BP1 during SGs assembly and/or blockade (Panas et al., 2012; Reineke and Lloyd, 2013; Valiente-Echeverria et al., 2014), we further investigated the nature of VP35 and G3BP1 interplay. Proximity ligation assay (PLA) produces distinct countable spots that represent a single-molecule protein interaction < 40 nm apart (Jarvius et al., 2007; Soderberg et al., 2006). In cells co-transfected with GFP-G3BP1 and MYC-VP35, we confirmed a close localization between G3BP1 and VP35 (53.3 ± 6.6

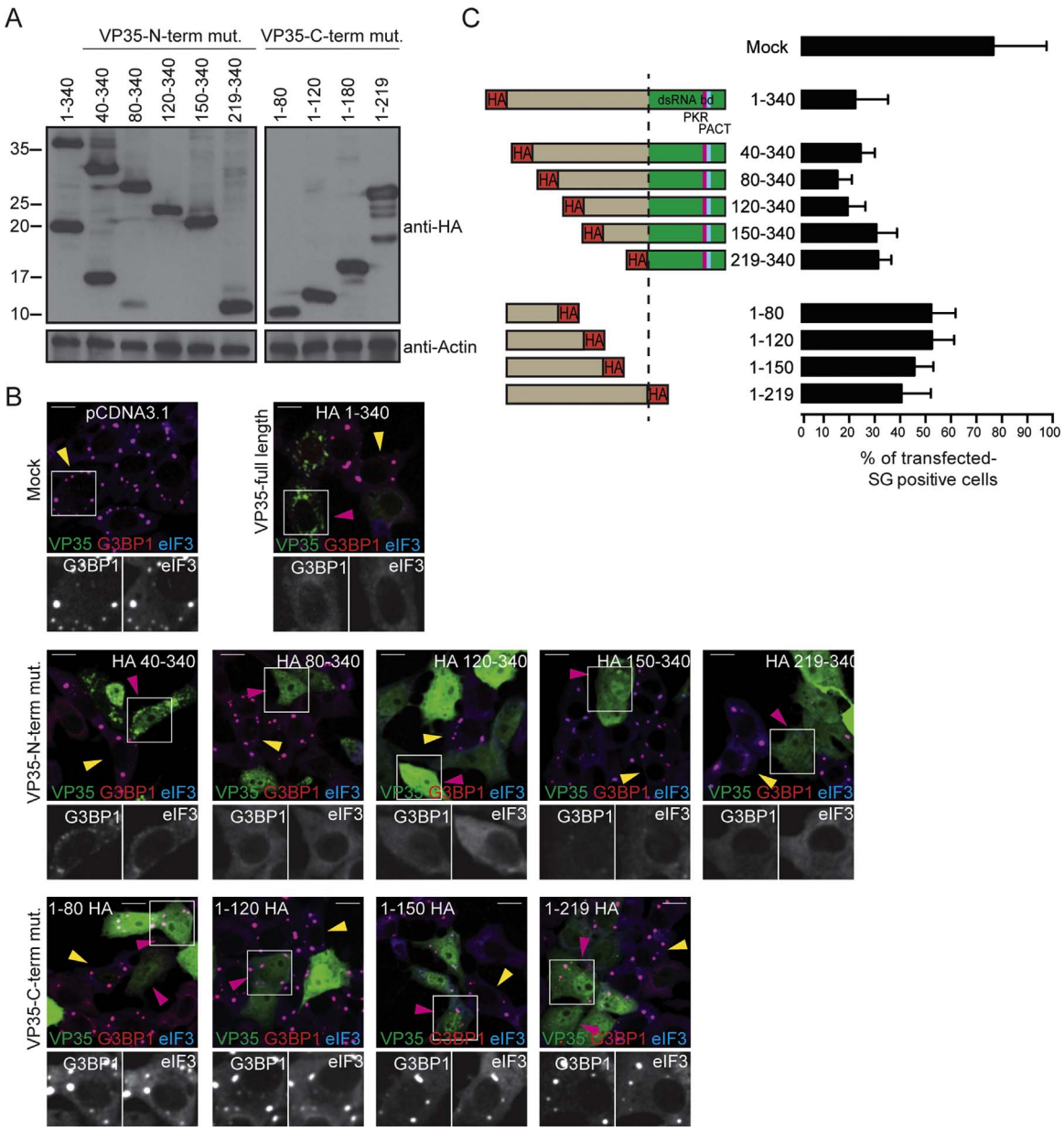

Fig. 6. The EBOV VP35 C-terminal domain is necessary for efficient SG clearance. (A) Vero cells were transfected with each of the indicated VP35 N- or C-terminal truncation mutants for 24 h. Cell lysates were collected, processed for Western blotting and probed for using anti-HA and actin antibodies. (B) Vero cells were transfected with each of the indicated VP35 N- or C-terminal truncation mutants for 24 h and left untreated (not shown) or treated with 500 μM Ars for 1 h. Cells were stained for HA (green), G3BP1 (red) and eIF3 (cyan). Yellow arrowheads indicate non-transfected cells, while pink arrowheads show VP35-expressing cells. Scale bars are 10 μm. Insets are individual channels on the boxed region. (C) Schematic diagram of HA-tagged VP35 N- or C-terminal truncation mutants. Quantification of cells exhibiting SGs derived from results shown in Panel 6 B. Error bars represent the standard deviation from three independent experiments with at least 150 cells counted per treatment.

spots), whereas there was little signal detected upon transfection of GFP-G3BP1 together with MYC tag only (5.1 ± 0.5 spots) (Fig. 5E and F). However, *in vitro* GST-pull down using recombinant G3BP1-GST (rG3BP1) and His-VP35 (rVP35) proteins revealed that rG3BP1 and rVP35 were unable to interact directly with each other (Fig. 4G). These results indicate that the G3BP1-VP35 interaction is indirect and requires another host factor(s) or only takes place under physiological conditions within a host cell.

3.7. The C-terminal of VP35 is necessary for inhibition of SG formation

VP35 has an N-terminal coiled-coil domain (amino acids 83–118), which is required for viral replication and nucleocapsid formation (Reid et al., 2005) and a C-terminal IID (amino acids 221–340) necessary for binding dsRNA and is sufficient for IFN inhibition (Basler et al., 2003; Cardenas et al., 2006; Hartman et al., 2004). To determine which domain of VP35 is required to block SG assembly, we transfected Vero cells with a series of HA-tagged N- and C-terminal VP35 truncations (Fig. 6A) and stressed with Ars. The N-terminal VP35 truncations, 40–340 and 80–340 had SGs in 24% and 14.7% of cells, respectively, and were found to associate and surround SGs upon treatment with Ars (Fig. 6B and C). Interestingly, constructs 120–340, 150–340 and 219–340 displayed a completely diffuse localization throughout the cytoplasm and visible SGs were present in 18.7%, 30% and 31% of cells, respectively (Fig. 6B and C). Deletion of the C-terminal domain (219–340) appeared to have a detrimental effect on the SG blockade, with 52.2%, 52.5%, 45.5% and 40.3% of cells expressing the truncation mutants 1–80, 1–120, 1–150 and 1–219 having SGs, respectively, but did not reach the 77% of mock-trans-

fected cells displaying SGs (Fig. 6B and C). We interpret this observation to suggest that the C-terminal domain of VP35 is required for the efficient inhibition of SG assembly. To link the binding of a particular SG component (eEF2, eIF3 or G3BP1) to a domain of VP35, we attempted to perform immunoprecipitations with the VP35 truncation mutants. Although the HA-tagged constructs (VP35 full length and truncations) were successfully pulled-down, non-specific binding of SG-marker specific proteins (e.g., G3BP1, eIF3 & eEF2) to the HA-beads rendered this experiment inconclusive (data not shown).

4. Discussion

A common feature of many RNA viruses is the transient induction of SG (Lloyd, 2013), which is triggered early upon generation of dsRNA replication intermediates, causing the activation of PKR and phosphorylation of eIF2α. Here, we demonstrate that ZEBOV trVLP infection does not induce the assembly of SGs itself but does block SG assembly induced by oxidative stress. These data are in agreement with a recently published study that performed EBOV infection of U2OS cells under BSL4 containment (Nelson et al., 2016). In our study, we demonstrate that EBOV VP35 is capable of blocking the assembly of both canonical and non-canonical SG induced by different kinds of stress, including that induced by Ars, PatA, Se and by the overexpression of TIA-1 or G3BP1, but not of those induced by PV infection. Moreover we demonstrated that EBOV VP35 pulls down different SG markers and indirectly, binds to G3BP1. Finally, the studies in which we employ VP35 truncation mutants suggest that the C-terminal region is required for inhibition of SG assembly.

The severe haemorrhagic fever caused by EBOV is characterized by early dysregulation of the host innate immune response through the sequestration of dsRNA by VP35. VP35 blocks PKR activation through its C-terminal IID by antagonizing and reversing PKR phosphorylation (Feng et al., 2007; Schumann et al., 2009). In untreated cells, there consistently appeared to be fewer cells with SGs and less phospho-eIF2α in those cells expressing VP35, which may be due to its activity on PKR. Yet, upon Ars stress the phosphorylation status of eIF2α was not reversed by VP35 (Fig. 2A and B) and instead suggests a mechanism of SG blockade that is eIF2α-independent. Moreover, VP35 does not appear to block SG assembly through the degradation of G3BP1, which is the case for PV at later times during infection (White et al., 2007) (Fig. 3D). Interestingly, VP35 is not able to counteract PV-triggered SG assembly (Supp. Fig. 1), which are compositionally distinct from the ones induced by oxidative stress, or heat shock, recruiting Sam68 but lacking eIF4G, PABP, and G3BP at later times (Piotrowska et al., 2010; White and Lloyd, 2011). It is possible that the differences in composition and mechanism of assembly of PV-induced SG granules displace key VP35-interacting partners and that the VP35 ability to block SG assembly is impaired in these conditions.

In SG-positive cells expressing low concentrations of VP35, we detected a distinct association of this viral protein with SGs (Figs. 1, 2 and 3). Taken together with the co-immunoprecipitation of multiple SG components with VP35 (Fig. 3A and D), we propose that a possible mechanism of SG dissolution relies on a VP35-mediated sequestration of a host protein that leads to a reduction in the number of SGs and a blockade in the host cell's ability to assemble new SGs with viral mRNAs. As the nucleation of SGs is driven by G3BP1 is response to stress (Tourriere et al., 2003), many viruses that induce SGs during infection have evolved countermeasures by targeting G3BP1 (Reineke and Lloyd, 2013). Several host and viral proteins containing an FGDF motif have been shown to interact with G3BP1 (Panas et al., 2015), although EBOV VP35 lacks this exact motif this does not strictly rule out binding as HIV-1 Gag also lacks this motif yet binds G3BP1 directly (Valiente-Echeverria et al., 2014). For example, different alphavirus non-structural proteins colocalize and co-immunoprecipitate with G3BP1 to sequester it in viral replication complexes (Cristea et al., 2006; Fros et al., 2012; Gorchakov et al., 2008; Panas et al., 2012). Here we clearly demonstrate that EBOV VP35 interacts with G3BP1 in co-immunoprecipitations and PLA; nevertheless, in vitro GST pull-down binding assays demonstrate that the interaction is likely to be indirect and may require another host factor or more physiological conditions (Fig. 5). Moreover, we observed a strong co-localization of G3BP1 and VP35 when both are diffusely distributed in the cytoplasm, supporting the hypothesis that VP35 blocks SG formation by recruiting fundamental SG components. Consistently, during trVLP infection SG components, such as TIAR (Fig. 1A), co-localize with EBOV VP35 in cytoplasmic aggregates, which are likely to be viral inclusion bodies (Nanbo et al., 2013) and may suggest that EBOV requires G3BP1 for replication similarly to Chikungunya virus that requires G3BP1 and G3BP2 to facilitate a switch from early to late stages of replication (Panas et al., 2015).

The HIV-1 structural protein Gag has been shown to interact with G3BP1 and eEF2 to dissolve SGs, which is critical for the block to SG assembly (Ohn et al., 2008; Valiente-Echeverria et al., 2014). HIV-1 also appears to be able to dissolve other forms of SGs such as those induced by selenite but through a mechanism that does not require eEF2 binding but instead affects the association of hypophosphorylated 4EBP1 to the mRNA cap to allow continued translation of Gag (Cinti et al., 2016; Emara et al., 2012). eEF2 is an important component in translation elongation and its phosphorylation enhances shutoff of mRNA translation in response to stress (Patel et al., 2002). Indeed, we have shown that VP35 co-immunoprecipitated with eEF2, however, we were unable to determine whether or not VP35 required eEF2 for SG repression. In Ars-treated, GFP-expressing cells, knockdown of eEF2 resulted in approximately 3% of cells having SGs (data not shown). This low percentage of SG positive cells made it difficult to conclude any additional effect of EBOV VP35 on SG blockade (data not shown). The canonical SG component eIF3 was also specifically pulled down by VP35 but did not appear to be essential for SG blockade as Se-induced SGs, that characteristically lack eIF3 (Fujimura et al., 2012), were still dissolved by the viral protein (Fig. 3). 100 host genes have been identified as being involved in SG assembly (Jain et al., 2016; Ohn et al., 2008), all of these serving to restrict or reprogram host gene expression predominantly to the disadvantage of the virus. More extensive work will be required to determine the exact mechanism of SG repression by EBOV VP35 and whether or not G3BP1/eEF2 binding is required for this activity.

The ability of EBOV VP35 to block SG assembly appeared to require, at least in part, its C-terminal region of which several high resolution structures are available (Leung et al., 2009, 2010a, 2010b). This domain contains important clusters of conserved basic residues necessary for protein-protein and protein-RNA interactions (Hastie et al., 2012). Although, we demonstrate that RNA does not mediate the interaction between eEF2 and eIF3 (Fig. 5D), the C-terminal domain of VP35 appears, at least in part, to be necessary for SG blockade (Fig. 6). Interestingly, amino acids 80–120, which contain the coiled coil domain, were not required for SG dissolution yet appeared to be necessary for the association to SGs in the presence of Ars but only in the context of the C-terminal domain (Fig. 6). This result suggests that the coiled coil domain may be necessary for binding to a particular SG component. More work will be required to clarify this point.

Recently published work complements the work presented here in that Nelson et al., using several of the techniques used herein, showed that VP35 subverts the host stress response by preventing type I SG assembly (Nelson et al., 2016), whereby threshold levels of VP35 were necessary to elicit this effect, similar to the conclusions reached here (Fig. 4). Likewise, VP35 coaggregated with several SG proteins including eIF3, eIF4G, PABP and TIAR (Nelson et al., 2016 and this work) in cytoplasmic inclusion bodies. Nevertheless, our work both complements and extends the study. For example, we demonstrate that VP35 blocks type II SGs that assemble via alternative mechanisms (Cinti et al., 2016; Fujimura et al., 2012). In addition, we employed in vitro

GST-pulldown as well as *in situ* (live cell) interaction assays to demonstrate interactions between VP35 with SG components (Fig. 5). Finally, we mapped the domain of VP35 that elicits the SG blockade to the C-terminal domain, a domain that binds double-stranded RNA (dsRNA) and antagonizes type I IFN responses and that therefore likely mediate innate responses to infection (Fig. 6). Nelson *et al.* also used an RNA binding point mutants of VP35 to determine if this activity was required. In the work presented here, a more severe truncation mutant lost the ability to suppress SG assembly, while full length VP35 did not require RNA to associate to SG components G3BP-1, eIF2 and eIF3, indicating that the inherent RNA-binding domain of VP35 may not be an absolute requirement for the SG blockade but may also require contributions of other VP35 domains.

In conclusion, we describe a novel activity of EBOV VP35 and another mechanism by which this viral protein inhibits the host innate immune response to block SG assembly when cells are exposed to different stressors. This work represents yet another example of an RNA virus that encodes a limited number of genes and that has evolved a mechanism to control SG assembly/function to potentially foster a productive replication environment.

Funding sources

This work was supported by grants MOP-38111 and MOP-56974 from the Canadian Institutes of Health Research (CIHR) to A.J.M. and by The Canadian HIV Cure Enterprise Team Grant HIG-133050 (to A.J.M.) from the CIHR in partnership with Canadian Foundation for HIV-1/AIDS Research and The International AIDS Society. RA is funded by a Conselho Nacional de Desenvolvimento Científico e Tecnológico Fellowship (Brazil). The funders had no role in study design, data collection and interpretation, or the decision to submit the work for publication.

Acknowledgement

We would like to thank Heinz Feldmann, Thomas Hoenen, Nancy Kedersha, Paul Anderson, Jerry Pelletier, Erica Saphire, Rongtuan Lin, Imed Gallouzi for generous provisions of cell lines and reagents and Meijuan Niu for technical help.

Appendix A. Supporting information

Supplementary data associated with this article can be found in the online version at doi:10.1016/j.virol.2016.12.012.

References

Anderson, P., Kedersha, N., 2002. Visibly stressed: the role of eIF2, TIA-1, and stress granules in protein translation. Cell Stress Chaperon. 7, 213–221.
Baize, S., Leroy, E.M., Georges-Courbot, M.C., Capron, M., Lansoud-Soukate, J., Debre, P., Fisher-Hoch, S.P., McCormick, J.B., Georges, A.J., 1999. Defective humoral responses and extensive intravascular apoptosis are associated with fatal outcome in Ebola virus-infected patients. Nat. Med. 5, 423–426.
Basler, C.F., Mikulasova, A., Martinez-Sobrido, L., Paragas, J., Muhlberger, E., Bray, M., Klenk, H.D., Palese, P., Garcia-Sastre, A., 2003. The Ebola virus VP35 protein inhibits activation of interferon regulatory factor 3. J. Virol. 77, 7945–7956.
Basler, C.F., Wang, X., Muhlberger, E., Volchkov, V., Paragas, J., Klenk, H.D., Garcia-Sastre, A., Palese, P., 2000. The Ebola virus VP35 protein functions as a type I IFN antagonist. Proc. Natl. Acad. Sci. USA 97, 12289–12294.
Buchan, J.R., Parker, R., 2009. Eukaryotic stress granules: the ins and outs of translation. Mol. Cell 36, 932–941.
Cardenas, W.B., Loo, Y.M., Gale, M., Jr., Hartman, A.L., Kimberlin, C.R., Martinez-Sobrido, L., Saphire, E.O., Basler, C.F., 2006. Ebola virus VP35 protein binds double-stranded RNA and inhibits alpha/beta interferon production induced by RIG-I signaling. J. Virol. 80, 5168–5178.
Cinti, A., Le Sage, V., Ghanem, M., Mouland, A.J., 2016. HIV-1 gag blocks selenite-induced stress granule assembly by altering the mRNA cap-binding complex. MBio, 7.
Cristea, I.M., Carroll, J.W., Rout, M.P., Rice, C.M., Chait, B.T., MacDonald, M.R., 2006. Tracking and elucidating alphavirus-host protein interactions. J. Biol. Chem. 281, 30269–30278.
Dang, Y., Kedersha, N., Low, W.K., Romo, D., Gorospe, M., Kaufman, R., Anderson, P., Liu, J.O., 2006. Eukaryotic initiation factor 2alpha-independent pathway of stress granule induction by the natural product pateamine A. J. Biol. Chem. 281, 32870–32878.
Dougherty, J.D., Tsai, W.C., Lloyd, R.E., 2015. Multiple Poliovirus Proteins Repress Cytoplasmic RNA Granules. Viruses 7, 6127–6140.
Emara, M.M., Fujimura, K., Sciaranghella, D., Ivanova, V., Ivanov, P., Anderson, P., 2012. Hydrogen peroxide induces stress granule formation independent of eIF2alpha phosphorylation. Biochem. Biophys. Res. Commun. 423, 763–769.
Fabozzi, G., Nabel, C.S., Dolan, M.A., Sullivan, N.J., 2011. Ebolavirus proteins suppress the effects of small interfering RNA by direct interaction with the mammalian RNA interference pathway. J. Virol. 85, 2512–2523.
Feng, Z., Cerveny, M., Yan, Z., He, B., 2007. The VP35 protein of Ebola virus inhibits the antiviral effect mediated by double-stranded RNA-dependent protein kinase PKR. J. Virol. 81, 182–192.
Fros, J.J., Domeradzka, N.E., Baggen, J., Geertsema, C., Flipse, J., Vlak, J.M., Pijlman, G.P., 2012. Chikungunya virus nsP3 blocks stress granule assembly by recruitment of G3BP into cytoplasmic foci. J. Virol. 86, 10873–10879.
Fujimura, K., Sasaki, A.T., Anderson, P., 2012. Selenite targets eIF4E-binding protein-1 to inhibit translation initiation and induce the assembly of non-canonical stress granules. Nucleic Acids Res. 40, 8099–8110.
Gilks, N., Kedersha, N., Ayodele, M., Shen, L., Stoecklin, G., Dember, L.M., Anderson, P., 2004. Stress granule assembly is mediated by prion-like aggregation of TIA-1. Mol. Biol. Cell 15, 5383–5398.
Gorchakov, R., Frolova, E., Sawicki, S., Atasheva, S., Sawicki, D., Frolov, I., 2008. A new role for ns polyprotein cleavage in Sindbis virus replication. J. Virol. 82, 6218–6231.
Haasnoot, J., de Vries, W., Geutjes, E.J., Prins, M., de Haan, P., Berkhout, B., 2007. The Ebola virus VP35 protein is a suppressor of RNA silencing. PLoS Pathog. 3, e86.
Harcourt, B.H., Sanchez, A., Offermann, M.K., 1998. Ebola virus inhibits induction of genes by double-stranded RNA in endothelial cells. Virology 252, 179–188.
Harcourt, B.H., Sanchez, A., Offermann, M.K., 1999. Ebola virus selectively inhibits responses to interferons, but not to interleukin-1beta, in endothelial cells. J. Virol. 73, 3491–3496.
Hartman, A.L., Towner, J.S., Nichol, S.T., 2004. A C-terminal basic amino acid motif of Zaire ebolavirus VP35 is essential for type I interferon antagonism and displays high identity with the RNA-binding domain of another interferon antagonist, the NS1 protein of influenza A virus. Virology 328, 177–184.
Hastie, K.M., Bale, S., Kimberlin, C.R., Saphire, E.O., 2012. Hiding the evidence: two strategies for innate immune evasion by hemorrhagic fever viruses. Curr. Opin. Virol. 2, 151–156.
Hoenen, T., Watt, A., Mora, A., Feldmann, H., 2014. Modeling the lifecycle of Ebola virus under biosafety level 2 conditions with virus-like particles containing tetracistronic minigenomes. J. Vis. Exp.: JoVE, 52381.
Huang, Y., Xu, L., Sun, Y., Nabel, G.J., 2002. The assembly of Ebola virus nucleocapsid requires virion-associated proteins 35 and 24 and posttranslational modification of nucleoprotein. Mol. Cell 10, 307–316.
Jain, S., Wheeler, J.R., Walters, R.W., Agrawal, A., Barsic, A., Parker, R., 2016. ATPase-Modulated Stress Granules Contain a Diverse Proteome and Substructure. Cell 164, 487–498.
Jarvius, M., Paulsson, J., Weibrecht, I., Leuchowius, K.J., Andersson, A.C., Wahlby, C., Gullberg, M., Botling, J., Sjoblom, T., Markova, B., Ostman, A., Landegren, U., Soderberg, O., 2007. In situ detection of phosphorylated platelet-derived growth factor receptor beta using a generalized proximity ligation method. Mol. Cell. Proteom.: MCP 6, 1500–1509.
Johnson, R.F., McCarthy, S.E., Godlewski, P.J., Harty, R.N., 2006. Ebola virus VP35-VP40 interaction is sufficient for packaging ^{3}E–^{5}E minigenome RNA into virus-like particles. J. Virol. 80, 5135–5144.
Kedersha, N., Cho, M.R., Li, W., Yacono, P.W., Chen, S., Gilks, N., Golan, D.E., Anderson, P., 2000. Dynamic shuttling of TIA-1 accompanies the recruitment of mRNA to mammalian stress granules. J. Cell Biol. 151, 1257–1268.
Kedersha, N.L., Gupta, M., Li, W., Miller, I., Anderson, P., 1999. RNA-binding proteins TIA-1 and TIAR link the phosphorylation of eIF-2 alpha to the assembly of mammalian stress granules. J. Cell Biol. 147, 1431–1442.
Kimberlin, C.R., Bornholdt, Z.A., Li, S., Woods, V.L., Jr., MacRae, I.J., Saphire, E.O., 2010. Ebolavirus VP35 uses a bimodal strategy to bind dsRNA for innate immune suppression. Proc. Natl. Acad. Sci. USA 107, 314–319.
Kirchdoerfer, R.N., Abelson, D.M., Li, S., Wood, M.R., Saphire, E.O., 2015. Assembly of the Ebola Virus Nucleoprotein from a Chaperoned VP35Complex. Cell Rep. 12, 140–149.
Leung, D.W., Ginder, N.D., Fulton, D.B., Nix, J., Basler, C.F., Honzatko, R.B., Amarasinghe, G.K., 2009. Structure of the Ebola VP35 interferon inhibitory domain. Proc. Natl. Acad. Sci. USA 106, 411–416.
Leung, D.W., Prins, K.C., Borek, D.M., Farahbakhsh, M., Tufariello, J.M., Ramanan, P., Nix, J.C., Helgeson, L.A., Otwinowski, Z., Honzatko, R.B., Basler, C.F., Amarasinghe, G.K., 2010a. Structural basis for dsRNA recognition and interferon antagonism by Ebola VP35. Nat. Struct. Mol. Biol. 17, 165–172.
Leung, D.W., Shabman, R.S., Farahbakhsh, M., Prins, K.C., Borek, D.M., Wang, T., Muhlberger, E., Basler, C.F., Amarasinghe, G.K., 2010b. Structural and functional characterization of Reston Ebola virus VP35 interferon inhibitory domain. J. Mol. Biol. 399, 347–357.
Lloyd, R.E., 2013. Regulation of stress granules and P-bodies during RNA virus infection. Wiley interdisciplinary reviews. RNA 4, 317–331.
Martinez, M.J., Salim, A.M., Hurtado, J.C., Kilgore, P.E., 2015. Ebola virus infection: overview and update on prevention and treatment. Infect. Dis. Ther. 4, 365–390.
McCarthy, S.D., Majchrzak-Kita, B., Racine, T., Kozlowski, H.N., Baker, D.P., Hoenen, T.,

Kobinger, G.P., Fish, E.N., Branch, D.R., 2016. A Rapid screening assay identifies monotherapy with interferon-ss and combination therapies with nucleoside analogs as effective inhibitors of Ebola virus. PLoS Negl. Trop. Dis. 10, e0004364.
Monette, A., Valiente-Echeverria, F., Rivero, M., Cohen, E.A., Lopez-Lastra, M., Mouland, A.J., 2013. Dual mechanisms of translation initiation of the full-length HIV-1 mRNA contribute to gag synthesis. PLoS One 8, e68108.
Muhlberger, E., Lotfering, B., Klenk, H.D., Becker, S., 1998. Three of the four nucleocapsid proteins of Marburg virus, NP, VP35, and L, are sufficient to mediate replication and transcription of Marburg virus-specific monocistronic minigenomes. J. Virol. 72, 8756–8764.
Nanbo, A., Watanabe, S., Halfmann, P., Kawaoka, Y., 2013. The spatio-temporal distribution dynamics of Ebola virus proteins and RNA in infected cells. Sci. Rep. 3, 1206.
Nelson, E.V., Schmidt, K.M., Deflube, L.R., Doganay, S., Banadyga, L., Olejnik, J., Hume, A.J., Ryabchikova, E., Ebihara, H., Kedersha, N., Ha, T., Muhlberger, E., 2016. Ebola virus does not induce stress granule formation during infection and sequesters stress granule proteins within viral inclusions. J. Virol..
Noda, T., Aoyama, K., Sagara, H., Kida, H., Kawaoka, Y., 2005. Nucleocapsid-like structures of Ebola virus reconstructed using electron tomography. J. Vet. Med. Sci./Jpn. Soc. Vet. Sci. 67, 325–328.
Ohn, T., Kedersha, N., Hickman, T., Tisdale, S., Anderson, P., 2008. A functional RNAi screen links O-GlcNAc modification of ribosomal proteins to stress granule and processing body assembly. Nat. Cell Biol. 10, 1224–1231.
Panas, M.D., Schulte, T., Thaa, B., Sandalova, T., Kedersha, N., Achour, A., McInerney, G.M., 2015. Viral and cellular proteins containing FGDF motifs bind G3BP to block stress granule formation. PLoS Pathog. 11, e1004659.
Panas, M.D., Varjak, M., Lulla, A., Eng, K.E., Merits, A., Karlsson Hedestam, G.B., McInerney, G.M., 2012. Sequestration of G3BP coupled with efficient translation inhibits stress granules in Semliki Forest virus infection. Mol. Biol. Cell 23, 4701–4712.
Patel, J., McLeod, L.E., Vries, R.G., Flynn, A., Wang, X., Proud, C.G., 2002. Cellular stresses profoundly inhibit protein synthesis and modulate the states of phosphorylation of multiple translation factors. Eur. J. Biochem. 269, 3076–3085.
Piotrowska, J., Hansen, S.J., Park, N., Jamka, K., Sarnow, P., Gustin, K.E., 2010. Stable formation of compositionally unique stress granules in virus-infected cells. J. Virol. 84, 3654–3665.
Poblete-Duran, N., Prades-Perez, Y., Vera-Otarola, J., Soto-Rifo, R., Valiente-Echeverria, F., 2016. Who regulates whom? An overview of RNA granules and viral infections. Viruses, 8.
Reid, S.P., Cardenas, W.B., Basler, C.F., 2005. Homo-oligomerization facilitates the interferon-antagonist activity of the ebolavirus VP35 protein. Virology 341, 179–189.
Reineke, L.C., Kedersha, N., Langereis, M.A., van Kuppeveld, F.J., Lloyd, R.E., 2015. Stress granules regulate double-stranded RNA-dependent protein kinase activation through a complex containing G3BP1 and Caprin1. MBio 6, e02486.
Reineke, L.C., Lloyd, R.E., 2013. Diversion of stress granules and P-bodies during viral infection. Virology 436, 255–267.
Reineke, L.C., Lloyd, R.E., 2015. The stress granule protein G3BP1 recruits protein kinase R to promote multiple innate immune antiviral responses. J. Virol. 89, 2575–2589.
Sanchez, A., Lukwiya, M., Bausch, D., Mahanty, S., Sanchez, A.J., Wagoner, K.D., Rollin, P.E., 2004. Analysis of human peripheral blood samples from fatal and nonfatal cases of Ebola (Sudan) hemorrhagic fever: cellular responses, virus load, and nitric oxide levels. J. Virol. 78, 10370–10377.
Schumann, M., Gantke, T., Muhlberger, E., 2009. Ebola virus VP35 antagonizes PKR activity through its C-terminal interferon inhibitory domain. J. Virol. 83, 8993–8997.
Soderberg, O., Gullberg, M., Jarvius, M., Ridderstrale, K., Leuchowius, K.J., Jarvius, J., Wester, K., Hydbring, P., Bahram, F., Larsson, L.G., Landegren, U., 2006. Direct observation of individual endogenous protein complexes in situ by proximity ligation. Nat. Methods 3, 995–1000.
Taupin, J.L., Tian, Q., Kedersha, N., Robertson, M., Anderson, P., 1995. The RNA-binding protein TIAR is translocated from the nucleus to the cytoplasm during Fas-mediated apoptotic cell death. Proc. Natl. Acad. Sci. USA 92, 1629–1633.
Tourriere, H., Chebli, K., Zekri, L., Courselaud, B., Blanchard, J.M., Bertrand, E., Tazi, J., 2003. The RasGAP-associated endoribonuclease G3BP assembles stress granules. J. Cell Biol. 160, 823–831.
Towner, J.S., Rollin, P.E., Bausch, D.G., Sanchez, A., Crary, S.M., Vincent, M., Lee, W.F., Spiropoulou, C.F., Ksiazek, T.G., Lukwiya, M., Kaducu, F., Downing, R., Nichol, S.T., 2004. Rapid diagnosis of Ebola hemorrhagic fever by reverse transcription-PCR in an outbreak setting and assessment of patient viral load as a predictor of outcome. J. Virol. 78, 4330–4341.
Tsai, W.C., Lloyd, R.E., 2014. Cytoplasmic RNA granules and viral infection. Annu. Rev. Virol. 1, 147–170.
Valiente-Echeverria, F., Melnychuk, L., Vyboh, K., Ajamian, L., Gallouzi, I.E., Bernard, N., Mouland, A.J., 2014. eEF2 and Ras-GAP SH3 domain-binding protein (G3BP1) modulate stress granule assembly during HIV-1 infection. Nat. Commun. 5, 4819.
Vyboh, K., Ajamian, L., Mouland, A.J., 2012. Detection of viral RNA by fluorescence in situ hybridization (FISH). J. Vis. Exp.: JoVE, e4002.
Watt, A., Moukambi, F., Banadyga, L., Groseth, A., Callison, J., Herwig, A., Ebihara, H., Feldmann, H., Hoenen, T., 2014. A novel life cycle modeling system for Ebola virus shows a genome length-dependent role of VP24 in virus infectivity. J. Virol. 88, 10511–10524.
White, J.P., Cardenas, A.M., Marissen, W.E., Lloyd, R.E., 2007. Inhibition of cytoplasmic mRNA stress granule formation by a viral proteinase. Cell Host Microbe 2, 295–305.
White, J.P., Lloyd, R.E., 2011. Poliovirus unlinks TIA1 aggregation and mRNA stress granule formation. J. Virol. 85, 12442–12454.
Zinzula, L., Esposito, F., Muhlberger, E., Trunschke, M., Conrad, D., Piano, D., Tramontano, E., 2009. Purification and functional characterization of the full length recombinant Ebola virus VP35 protein expressed in E. coli. Protein Expr. Purif. 66, 113–119.